Nano Research 2018, 11(4): 1938–1955
https://doi.org/10.1007/s12274-017-1811-0
Research Article
ISSN 1998-0124
CN 11-5974/O4

A low-cost, printable, and stretchable strain sensor based on highly conductive elastic composites with tunable sensitivity for human motion monitoring

Yougen Hu[1], Tao Zhao[1], Pengli Zhu[1] (✉), Yuan Zhang[1,2], Xianwen Liang[1], Rong Sun[1] (✉), and Ching-Ping Wong[3,4]

[1] *Guangdong Provincial Key Laboratory of Materials for High Density Electronic Packaging, Shenzhen Institutes of Advanced Technology, Chinese Academy of Sciences, Shenzhen 518055, China*
[2] *Nano Science and Technology Institute, University of Science and Technology of China, Suzhou 215123, China*
[3] *School of Materials Science and Engineering, Georgia Institute of Technology, Atlanta, Georgia 30332, USA*
[4] *Department of Electronic Engineering, The Chinese University of Hong Kong, Hong Kong 999077, China*

Received: 6 June 2017
Revised: 8 August 2017
Accepted: 20 August 2017

KEYWORDS
flexible strain sensor, printable electronics, human motion monitoring, conductive elastic composites, silver-coated polymer spheres

ABSTRACT

Strain sensors with high stretchability, broad strain range, high sensitivity, and good reliability are desirable, owing to their promising applications in electronic skins and human motion monitoring systems. In this paper, we report a high-performance strain sensor based on printable and stretchable electrically conductive elastic composites. This strain sensor is fabricated by mixing silver-coated polystyrene spheres (PS@Ag) and liquid polydimethylsiloxane (PDMS) and screen-printed to a desirable geometry. The strain sensor exhibits fascinating comprehensive performances, including high electrical conductivity (1.65 × 104 S/m), large workable strain range (> 80%), high sensitivity (gauge factor of 17.5 in strain of 0%–10%, 6.0 in strain of 10%–60% and 78.6 in strain of 60%–80%), inconspicuous resistance overshoot (< 15%), good reproducibility and excellent long-term stability (1,750 h at 85 ˚C/85% relative humidity) for PS@Ag/PDMS-60, which only contains ~ 36.7 wt.% of silver. Simultaneously, this strain sensor provides the advantages of low-cost, simple, and large-area scalable fabrication, as well as robust mechanical properties and versatility in applications. Based on these performance characteristics, its applications in flexible printed electrodes and monitoring vigorous human motions are demonstrated, revealing its tremendous potential for applications in flexible and wearable electronics.

1 Introduction

Flexible and stretchable conductive materials have received significant attention in several applications such as flexible circuits [1–3], strain sensors [4–8], electronic skins [9–11], actuators [12], and wearable smart textile systems [13–15], because of their high mechanical deformation capability. Monitoring human

Address correspondence to Pengli Zhu, pl.zhu@siat.ac.cn; Rong Sun, rong.sun@siat.ac.cn

physiological signals is considered to be an effective approach for health assessment and disease diagnosis [16–18]. Strain sensors are often mounted on the human body or wearable equipment by integrating them with power sources [19]. Highly stretchable and sensitive strain sensors are required for the precise detection of human body activities, such as joint movements of the fingers, hands, arms, and legs, which usually result in ~ 50% strain. For example, Ryu et al. [20] reported an ultrahigh stretchability (> 900%) and a wearable strain sensor with high sensitivity, fabricated from dry-spun carbon nanotube (CNT) fibers, which can detect various human motions such as grasping and knee joint bending. Yoon et al. [21] presented a microfluidic strain sensor with high stretchability, sensitivity, and long-term stability and no considerable hysteresis by introducing a refractive-index matched ionic liquid into microfluidic networks embedded in an elastomeric matrix. These strain sensors were successfully used for monitoring a wide range of human body motions in real time. However, apart from the complicated fabrication process of these strain sensors, they exhibit very low electrical conductivity (or high initial resistance). This is detrimental to their practical applications, owing to the poor conductive performance of the strain sensors, which implies that a high supply power is needed. To simultaneously achieve high electrical conductivity and good stretchability, much effort has been devoted to creating compliant structural layouts, such as snake-like metal patterns on elastomeric substrates or buckled metal films on pre-strained elastomers, which are able to endure significant in-plane and out-of-plane deformation [22]. However, an obvious drawback of this approach is that it usually requires complicated design and manufacturing procedures. An alternative approach to achieve this target is to fabricate a blend by mixing conductive materials, such as metallic fillers, CNTs, or graphene, with a suitable elastic matrix. In this type of strain sensor, conductive fillers provide conductivity, while the elastomer endows the material with stretchability. A rather high filler loading (namely, high percolation threshold) is usually necessary to obtain satisfactory electrical properties. As a result, the dense conductive pathways throughout the polymer matrix might result in poor sensitivity, weak mechanical flexibility, and high cost.

To address these issues, constructing a conductive network with a low percolation threshold is a promising and effective approach to fabricate a highly flexible, stretchable, and sensitive strain sensor. Amjadi and co-workers [23] reported highly flexible, stretchable, and sensitive strain sensors based on nanocomposites with a silver nanowire (AgNW) network and polydimethylsiloxane (PDMS) elastomer in the form of a sandwich structure. The strain sensors exhibited a relatively low initial resistance of 7.5–246 Ω with different AgNW loadings, and simultaneously maintained high strain (70%) and high sensitivity (gauge factor of 2–14). Although these sandwiched AgNW sensors show good stretchability and sensitivity, the fabrication process is time-consuming and not scalable. Developing printable conductive elastic composites is one particularly promising solution for strain sensors, because printing technology is an effective way to fabricate low-cost and large-area electronics. Song et al. [24] demonstrated a printable microscale cracked strain sensor (PMSCSS) by screen-printing with a formulated ink based on carbon black. The PMSCSS shows high sensitivity with a gauge factor of 647; however, it has a large (megaohm-scale) initial resistance, and can be only used to detect an extremely small tensile strain within 0.51%. Therefore, up to now, the development of stretchable strain sensors that exhibit high electrical conductivity, stretchability, and sensitivity, and which have a simple and low-cost fabrication process is still a great challenge.

Herein, we present a facile and low-cost strategy to fabricate large-area, stretchable, and printable conductive elastic composite of PS@Ag/PDMS by simply mixing core–shell structured PS@Ag hybrids with a PDMS matrix, without any solvent addition. The highly stretchable and conductive PS@Ag/PDMS composite is then fabricated into flexible electrodes and strain sensors using printing technology. Owing to the unique core–shell conductive network structure of the composite, the percolation threshold is much smaller than that for conventional conductive polymer composites based on silver nanoparticles or silver flakes. The composite simultaneously exhibits high electrical conductivity (1.65×10^4 S/m), large workable strain range (> 80%), high sensitivity (gauge factor of 17.5 at

strains of 0%–10%, 6.0 at strains of 10%–60%, and 78.6 at strains of 60%–80%) and excellent long-term stability (1,750 h at 85 ℃/85% relative humidity (RH)) for PS@Ag/PDMS-60, which contains only ~ 36.7 wt.% of silver. Moreover, the electrical conductivity, breaking elongation, and sensitivity could be easily tunable by tailoring the PS@Ag filler loading. Based on the superior performance, the potential applications of this strain sensor in fabricating flexible electrodes or monitoring human motion, such as bending of the finger, wrist, and knee are further demonstrated.

2 Results and discussion

2.1 The electrical conductivity performance of the PS@Ag/PDMS composites

Figure 1(a) shows the electrical conductivity (σ) of the PS@Ag/PDMS composites with different PS@Ag filler loadings. The corresponding volume fractions of PS@Ag and actual Ag content were calculated from the mass fractions of the PS@Ag filler and are listed in Table S1 in the Electronic Supplementary Material (ESM). An enhanced σ with increasing filler content is clearly observed and reaches a maximum value of 4.12×10^4 S/m at a PS@Ag loading of 50.77 vol.%, corresponding to an actual Ag mass fraction of 42.84 wt.%. The exponential increase in the electrical conductivity of the composites above the percolation threshold (green line) can be observed, and these empirical data are consistent with the classical percolation theory expressed by the power law relationship as follows [25]

$$\sigma = \sigma_0(\phi - \phi_c)^t \quad (1)$$

where σ_0 is the proportionality constant related to the intrinsic conductivity of the conductive filler, ϕ is the volume fraction of the filler, ϕ_c is the critical volume fraction of the filler at percolation, and t is the critical exponent relating to the system dimensionality of composites. Percolation in the composites does occur when the PS@Ag content is 25.77 vol.% (i.e., 3.5 vol.% or 26.9 wt.% of Ag) according to the fitted data, which is close to the empirically derived value of 27 vol.% found for random close-packed structures made using balls of the continuum percolation model [26]. The percolation value of 26.9 wt.% for the actual Ag in our PS@Ag/PDMS composites is 50% lower than that of the ~ 60 wt.% in Ag-PDMS composites reported by Larmagnac et al. [27], which use pure silver powder with a size of 2–3.5 μm as the conductive filler. Furthermore, for the samples to have the same conductivity, such as 300 S/m, a heavy Ag loading of ~ 77 wt.% in Ag-PDMS is required; nevertheless, only ~ 40 wt.% of Ag is required in our PS@Ag/PDMS samples. This clearly indicates that this type of metal-coated polymer conductive hybrid can significantly reduce the consumption of silver, along with the cost of the ultimate products. To make a more detailed comparison, the maximum electrical conductivity and percolation threshold data of the recently reported conductive composites are summarized in Table S2 in the ESM. This comparison shows that the PS@Ag/PDMS composites possess a much better percolation probability than their pure metal-based counterparts, and also exhibit high conductivity. Obviously, the outstanding conductivity and low percolation threshold value benefit considerably from the three-dimensional (3D) core–shell structure of the PS@Ag conductive filler in the PDMS matrix, because it exhibits conductivity as an electrical percolation system in an effective way. In other words, the conductive filler forms connected pathways through the silver coating on the PS microspheres with its content as low as possible. The inset in Fig. 1(a) shows the best regression fits using the power law relationship. The critical exponent t in the power law relationship is a parameter related to the microstructural properties of the composites [28]. It is found that t = 1.57, which is in agreement with the critical conduction behavior for 3D network systems of conductive spherical particles in an insulating matrix, where the values of t are in the range 1.5–2.0 [26]. Figures 1(b)–1(e) show the representative cross-section morphology of PS@Ag/PDMS films with different filler contents. On gradually increasing the PS@Ag loading from 15.92 vol.% (Fig. 1(b)) to 30.65 vol.% (Fig. 1(c)) and 50.77 vol.% (Fig. 1(d)), the conductive pathways correspondingly increase, resulting in the transformation from an insulating to a conductive state of the PS@Ag/PDMS composites. The magnified scanning electron microscopy (SEM) image in Fig. 1(e) reveals good contacts among neighboring fillers and

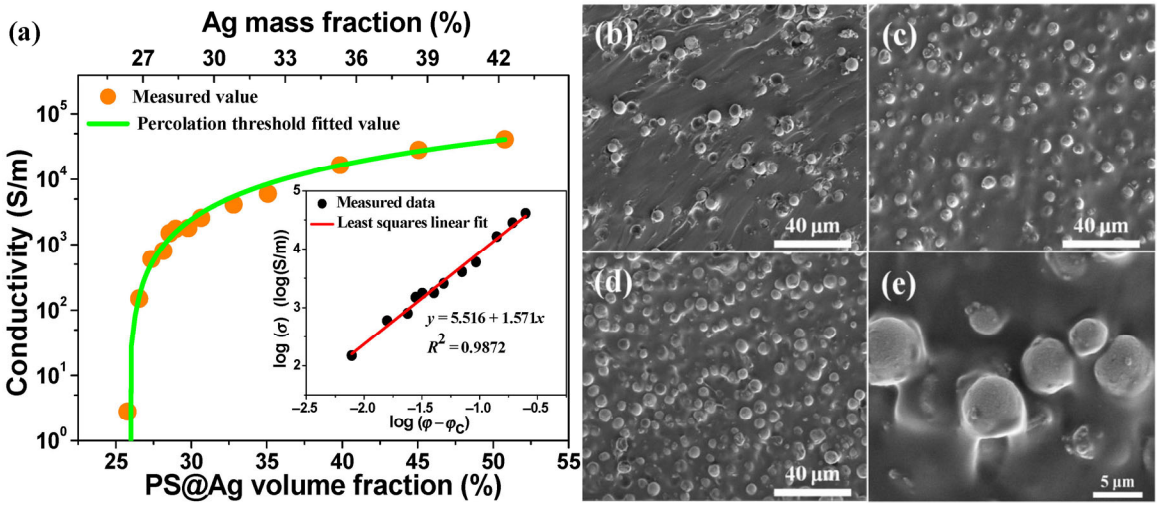

Figure 1 (a) Electrical conductivity of the PS@Ag/PDMS composites as a function of filler loading. Inset is the linear fitting of the data to the power law equation for electrical conductivity. The cross-sectional SEM images of representative PS@Ag/PDMS films with different PS@Ag filler loadings of (b) 15.92 vol.% (30 wt.%), (c) 30.65 vol.% (50 wt.%), and ((d) and (e)) 50.77 vol.% (70 wt.%), respectively.

excellent interfacial adhesion between PS@Ag particles and the PDMS matrix. This high-filler loading provides sufficient conductive paths for the PS@Ag/PDMS composites and leads to high electrical conductivity.

2.2 The mechanical properties of the PS@Ag/PDMS composites

To demonstrate the mechanical flexibility of PS@Ag/PDMS film, it was stretched, twisted, and curled. As shown in Figs. 2(a)–2(d), the film exhibits outstanding elasticity and strength, thus holding great potential as a stretchable conductor and strain sensor upon the mechanical deformations. To determine the applications of the PS@Ag/PDMS in stretchable electronics, the PS@Ag/PDMS films with various filler contents were mounted in the electronic universal tester and stretched to their maximum length to test their elongation capability. Figure 2(e) shows the stress–strain curves, and the strain is defined as $\varepsilon = (l - l_0)/l_0$, where l_0 is the initial length, and l is the length at different elongations. The stress represents as the ratio of tensile load and original cross-section area of films at $\varepsilon = 0$. It can be seen that the stress gradually increases with the increase in strain until the samples rupture. The maximum strains of the samples at breaking point are shown in Fig. 2(f) (blue column). It shows that the strain at rupture decreases with the increase in filler content, implying more PS@Ag filler will probably lead to more fragile films. In detail, the pure PDMS films without addition of PS@Ag filler could be stretched to 155% of maximum strain at rupture, indicating high stretch ability of the PDMS film. When a relatively small amount of 30 wt.% PS@Ag filler was added, the elongation at break was slightly reduced to 140%. As the PS@Ag filler loading was increased to a medium value, such as 55 wt.%, the elongation at rupture of sample decreased to ~ 91.5%. Moreover, when the PS@Ag filler content was further increased to 70 wt.%, the strain at break of PS@Ag/PDMS film was approximately 72%. Although this elongation at break is obviously lower compared with the pristine PDMS sample, the conductive composites still possess excellent stretchability under such particularly high filler content. The elastic modulus defined as the slope for the first 2% strain is calculated by a linear fitting of the initial linear elastic region (inset in Fig. 2(e)) and plotted against the PS@Ag filler content, as shown in Fig. 2(f) (red column). The elastic modulus increased nearly four-fold, from 0.468 to 2.19 MPa, as the filler content increased from 0 to 70 wt.%, indicating an expected increase in the stiffness of PS@Ag/PDMS films after introducing the PS@Ag

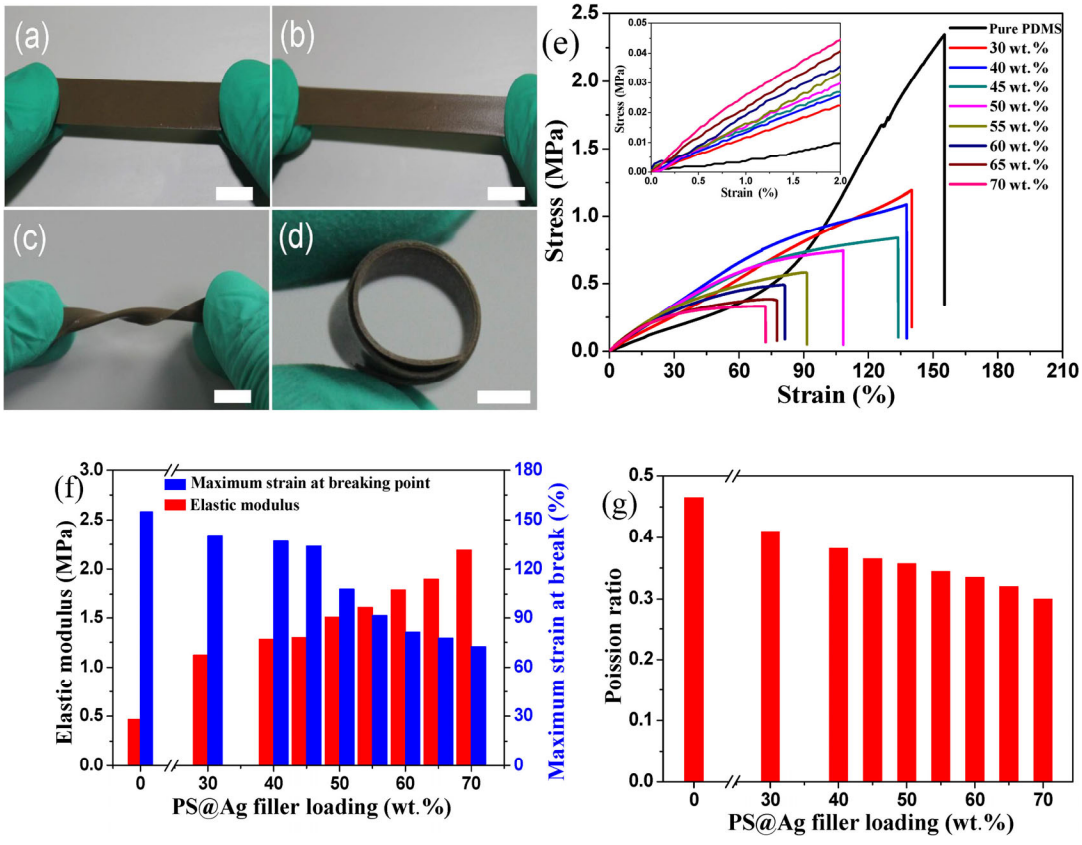

Figure 2 Photographs of a PS@Ag/PDMS film under different deformations: (a) initial state, (b) stretching, (c) twisting, and (d) curling, respectively. The scale bars indicate 1 cm. (e) Stress–strain curves, (f) elastic modulus and maximum strain at break, and (g) Poisson's ratio of the PS@Ag/PDMS films with different filler loadings, respectively.

filler. To investigate the changes in Poisson's ratio (ν) with filer content, PS@Ag/PDMS films were fixed on a custom-made manual stretcher and measured with an optical microscope by observing the same locations as depicted in Fig. S1 in the ESM. Figure 2(g) demonstrates Poisson's ratio is lower with higher PS@Ag filler content. Pure PDMS elastomer is generally considered to be incompressible with a value of ν = 0.5. Increasing the amount of filler decreased the Poisson's ratio, probably attributable to dewetting and vacuole formation due to relatively weak bonding between the PS@Ag particles and PDMS matrix.

To assess the recyclable stretchability of PS@Ag/PDMS films, sets of stretch and recovery tests were conducted for 30 cycles with maximum strains of 10%, 30%, and 50%, and the cyclic stress–strain curves were collected, as shown in Figs. S2(a)–S2(f) in the ESM. As can be seen, the stress–strain curves are strongly dependent on the strain level. Pure PDMS film presents approximately linear stretch–recovery paths for 10%, 30%, and 50% strain after 30 cycles. The strain of recovery curves could almost return to the original points after relaxing for each strain, indicating that PDMS film could completely recover to their original size with good elastic deformation. However, for PS@Ag/PDMS films, hysteresis phenomena are observed in the cyclic stretch and recovery paths of the stress–strain curves, especially for the first loading and unloading paths of the curves of the films with high strain and high filler loading. After the first cyclic test, the hysteresis phenomenon reduces greatly and the stress–strain curves gradually converge to a relatively stable hysteresis loop during the cyclic stretch tests. The results reveal that after only a small number of cycles, the majority of the elongation has taken place, with the films exhibiting a nearly steady-state response for further cycles. This stress-softening phenomenon is typical for filled silicon rubber materials, and is

known as the Mullins effect [29].

2.3 The electromechanical behavior of the PS@Ag/PDMS composites

The electrical property of the PS@Ag/PDMS films is anticipated to be influenced by the mechanical behavior owing to the changes in the conductive paths in the flexible PDMS matrix. Good electromechanical behavior is greatly desirable for use as stretchable conductors or elastic strain sensors. The resistance change ratio $\Delta R/R_0$ (R_0 is the initial electrical resistance and ΔR is the electrical resistance change at a specified strain level) as a function of quasi-static uniaxial strain is measured to maximum elongation to study the strain-sensing behavior of PS@Ag/PDMS conductive composites. As shown in Figs. 3(a)–3(d), the $\Delta R/R_0$ values of the PS@Ag/PDMS films increase with increasing strain until the cracking occurred. The most interesting feature here is that $\Delta R/R_0$ is intimately related to the filler content under strain tension. The PS@Ag/PDMS-70 and PS@Ag/PDMS-65 films show robust and excellent electrical properties, whereby under large maximum strains of ~ 72% and ~ 77%, the resistances increase almost linearly by only 4.41 and 6.88 times as compared with the original values, respectively (Fig. 3(a)). In other words, the stretchable PS@Ag/PDMS conductive films with above 65 wt.% filler loading maintained excellent electrical conductivity until the films ruptured. To express this in a more authentic way, a simple circuit consisting of a red-colored light-emitting diode (LED) is connected with the PS@Ag/PDMS-65 film to visually confirm the preservation of the electrical property of the film under high strain (Video S1 in the ESM). The LED shows stable luminescence even though the PS@Ag/PDMS film was stretched to near its maximum strain of rupture and turn off suddenly when the film rupture occurred (Fig. 3(e)), which demonstrates that the resistance increase of the flexible conductive film under the applied tensile strain is weak and insufficient to influence the illumination of the LED. Therefore, these films have potential applications in stretchable and flexible conductors, owing to their excellent performance in terms of maximum strain and electrical conductivity. For the PS@Ag/PDMS-60, PS@Ag/PDMS-55, and PS@Ag/PDMS-50 films, the resistances rapidly increase, particularly in the high-strain region near the maximum strain of rupture, as shown in Figs. 3(b)–3(d). The resistance of the PS@Ag/PDMS-60 film increased 1.75 times with a relatively steep gradient in the first 10% strain. The value of $\Delta R/R_0$ gradually increased to 9.86 with a relatively flat slope until the strain reached 70%, and then rapidly increased to 23.8 as the strain increased further to the breaking point of ~ 81%. Similar to PS@Ag/PDMS-60, PS@Ag/PDMS-55 exhibited a mild resistance increase before 60% strain and then a dramatic increase to 300 at the fracture point of ~ 90% strain. When the PS@Ag conductive filler further decreased to 50 wt.%, a distinctive variation could be observed. The value of $\Delta R/R_0$ increased logarithmically to approximately 2,000 under a low strain of approximately 37%, and then sharply increased by hundreds of times to the maximum measured value of the test equipment within a little more strain. The current–voltage (I–V) behaviors of two typical films, PS@Ag/PDMS-65 and PS@Ag/PDMS-55, are shown in Figs. 3(f) and 3(g). The currents increase linearly with voltage for the samples not only under no strain but also under various stretching states. The linear I–V characteristics reveal the excellent Ohmic behavior of the PS@Ag/PDMS films, which is very desirable for their applications as strain sensors. The slopes of the I–V curves decrease with increasing tensile strain, indicating that the resistances of the PS@Ag/PDMS conductive elastic films increase with the strains, i.e., the resistance is inversely proportional to the slope according to the Ohm's law. It also can be seen that the slopes of the PS@Ag/PDMS-65 film are obviously larger than that of the PS@Ag/PDMS-55 film under initial state even though it was stretched to 60% of strain, suggesting the resistance of PS@Ag/PDMS-65 film is much smaller than that of PS@Ag/PDMS-55. Moreover, the decreasing rate of the slope of the PS@Ag/PDMS-65 film is slower than that of PS@Ag/PDMS-55 film when they are gradually stretched from the initial state to 60% of strain, showing that the resistance increasing rate of the PS@Ag/PDMS-55 film is faster than that of the PS@Ag/PDMS-65 film during the stretching process. In other words, the PS@Ag/PDMS films containing fewer PS@Ag hybrid conductive particles exhibit larger resistances than those of films containing more

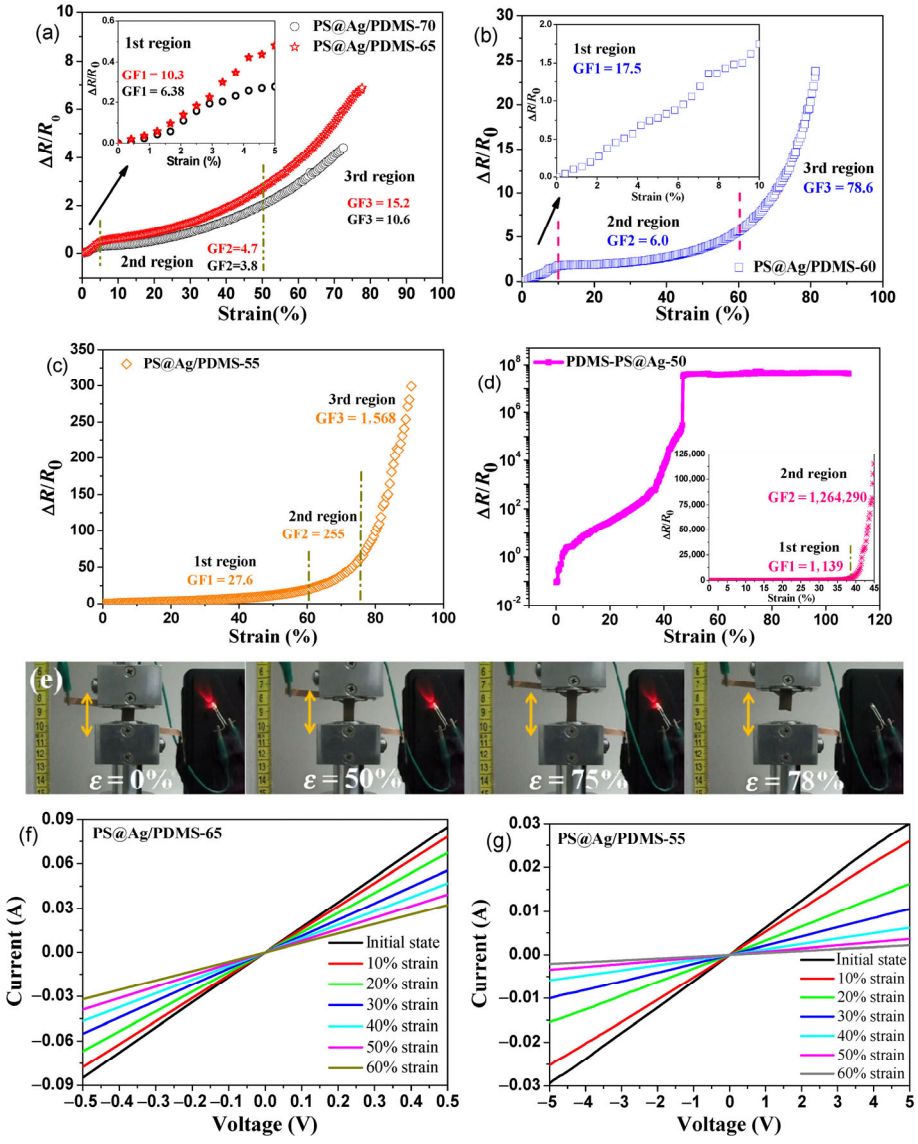

Figure 3 Electromechanical responses of the PS@Ag/PDMS strain sensors. (a)–(d) Relative change of resistance versus strain for the sensors with different filler loadings. (e) Digital photographs of LED lighting demonstration under various elongations for PS@Ag/PDMS-65 sensor. The brown arrows in the photographs represent the stretching direction. (f) and (g) Current–voltage curves of the PS@Ag/PDMS-65 and PS@Ag/PDMS-55 strain sensors for different levels of strains, respectively.

conductive fillers, and the former is more sensitive to the stretching strains. These *I*–*V* results are in accordance with the previous results shown in Figs. 1, 3(a), and 3(c).

The sensitivity of these strain sensors is thought to be one of the most important issues, because different applications often required different strain sensitivities. For a quantitative analysis of the strain sensitivity of the PS@Ag/PDMS conductive films, the strain gauge factor (GF), defined as GF = $(\Delta R/R_0)/\varepsilon$, is calculated. When the filler volume fraction is well above the percolation threshold, the GF values are strongly dependent on the stretch strain: 6.38 and 10.3 (ε = 0%–5%), 3.8 and 4.7 (ε = 5%–50%), and 10.6 and 15.2 (ε = 50%–maximum fracture strain) for the PS@Ag/PDMS-70 and PS@Ag/PDMS-65 films, respectively, and 17.5 (ε = 0%–10%), 6.0 (ε = 10%–60%), and 78.6 (ε = 50%–maximum fracture strain) for the PS@Ag/PDMS-60 film, as shown in Figs. 3(a) and 3(b) and their magnified insets. In the first region, the GF values

of the films increase sharply, owing to the sudden loss of most of the current paths of the PS@Ag conductive networks in the PDMS matrix along the strain direction. However, beyond the critical strain, the slope decreases as compared with the first region. This decreasing tendency originates from the fact that the rate of decrease in the number of current paths in the PDMS matrix is partly alleviated by the creation of new current paths perpendicular to the strain direction, probably due to the Poisson effect (compression in the perpendicular direction). The GF values then increase with further increases in the strain because the conductive paths are destroyed and reduced by physical cracking of the samples, especially near the maximum strain of fracture. When the filler volume fraction is slightly above the percolation threshold, such as the PS@Ag/PDMS-55 and PS@Ag/PDMS-50 films shown in Figs. 3(c) and 3(d), they exhibit remarkably large variation in the GF values. During the entire stretching process, the GF values are 27.6 (ε = 0%–60%), 255 (ε = 60%–75%), and 1,568 (ε = 75% to fracture strain of ~ 90%) for the PS@Ag/PDMS-55 film. Surprisingly, when the filler content was reduced to 50 wt.%, the GF value was high at 1,139 in a relatively low strain (ε = 0%–37%) and then radically increased to 1,264,290 in a very narrow range of strain (ε = 37%–45%). All the GF values and the corresponding correlation coefficients of the linear fitting are summarized in Table S3 in the ESM. A classical conductor–insulator transition is observed when an increasing stretching strain is loaded to a PS@Ag/PDMS-50 film. The large variance in the resistance and GF values of the PS@Ag/PDMS-50 film may be attributable to significant variation in the number and lengths of conduction paths formed by fillers (e.g., loss of contact among fillers) and tunneling resistance changes in neighboring fillers due to distance changes. According to the threshold theory, the resistance at low volume fractions, especially at volume fractions near to the percolation threshold, is dominated by tunneling resistance, and it is extremely sensitive to the gap width and the height of the potential barrier to be penetrated. Owing to this tunneling effect, the resistance logarithmically increases when the average distance between PS@Ag particles increases during the stretching procedure, as shown in Fig. 3(d). These results clearly indicate that the initial electrical conductivity (σ_0) and sensitivity (GF) of stretchable PS@Ag/PDMS composites can be easily tuned by controlling the PS@Ag filler content. The σ_0 enhances with increased filler loading, whereas GF is opposite, particularly for the samples with filler loading near the percolation threshold. The GF values of the stretchable PS@Ag/PDMS films are obviously higher than the classical metallic conductors (copper, nickel) of ~ 2 at the maximum (see "strain dependence of resistance for conductivity-invariant materials" in the ESM), and overcome the strain limits of traditional metal strain gauges (typically ~ 5%) with the piezoresistive principle, which have promising applications in strain sensors.

A description of the transport mechanism in terms of tunneling conduction between particles is proposed to explain the observed experimental results. The total electrical resistance of conductor-filled polymer composite is a function of both the resistance of each conducting particle and of the polymer matrix. As the conductivity of the particle is much larger as compared with that of the polymer matrix, the resistance across the particle may be neglected. When particles are separated far enough from each other, no current flows through the composite. If the distances between the particles are small, tunneling currents may arise. According to the model derived from tunneling theory by Simmons et al. [30, 31], the total electrical resistance R of the composite can be calculated as

$$R = \left(\frac{L}{N}\right)\left(\frac{8hs}{3\alpha^2\gamma\varepsilon^2}\right)\exp(\gamma s) \quad (2)$$

$$\gamma = \frac{4\pi}{h}\sqrt{2m\phi} \quad (3)$$

where L is the number of particles forming a single conducting path, N is the number of conducting paths, h is Plank's constant, s is the smallest distance between conductive particles, α^2 is the effective cross-section where tunneling occurs, e is the electron charge, m is the electron mass, and ϕ is the height of the potential barrier between adjacent particles. If strain is applied to the composite, the resistance will be altered owing to the change in particle separation. Assuming that under applied strain, the particle

separation changes from s_0 to s, and the number of conducting paths decreases from N_0 to N, the relative resistance (R/R_0) is given by

$$\frac{R}{R_0}=\left(\frac{Ns}{N_0 s_0}\right)\exp[\gamma(s-s_0)] \quad (4)$$

where R_0 is the initial resistance and s_0 is the initial inter-particle distance at zero strain. In case of elastic composites, the inter-particle distances under stretch strain is calculated as

$$s=s_0\left(1+\frac{\Delta l}{l_0}\right)=s_0(1+\varepsilon) \quad (5)$$

where l_0, Δl, and ε are the initial length, deformation, and stretch strain of the composite sample, respectively. In our case, it should be considered that ε is also related to the destruction of the conducting network because of the larger deformation of the elastic PDMS matrix, compared to rigid and immobilizing matrices, under stretching, and leads to a decrease in the number of conducting paths N

$$N=\frac{N_0}{\exp[A_1(\Delta l/l_0)+B_1(\Delta l/l_0)^2]}=\frac{N_0}{\exp(A_1\varepsilon+B_1\varepsilon^2)} \quad (6)$$

where N_0 is the initial number of conducting paths, and A_1 and B_1 are constants. Substitution of Eq. (5) and Eq. (6) into Eq. (4) yields

$$\frac{R}{R_0}=(1+\varepsilon)\exp(A\varepsilon+B\varepsilon^2) \quad (7)$$

where $A=\gamma s-A_1$, $B=-B_1$. The experimental data shown in Fig. 3 are compared to Eq. (7) and the fitted results are collected in Fig. S3 in the ESM. Apparently, a good agreement between the theoretical and experimental data is achieved. The difference between these fitting constant values is mainly due to the dissimilar deformation degrees of the composites with different filler content under stretching. The experimental results over all stretching ranges can be fitted well using the tunneling conduction model, suggesting that the tunneling mechanism is dominant for the transport of charge carriers in the composites under applied strain.

To investigate the cyclic stability of the strain sensors, the PS@Ag/PDMS-70 and PS@Ag/PDMS-50 films were representatively selected to test the resistance under repeated cycles of stretching/releasing with a given maximum strain. As shown in Fig. 4(a), the PS@Ag/PDMS-70 strain sensor exhibits a slight hysteretic behavior at the stretching/releasing cycle with a maximum strain of 10%, 30%, and 50%, possibly due to its viscoelastic property (Fig. S2(f) in the ESM). However, the strain-dependent responses are fully stabilized early on after five cycles for various loading strain values, which clearly indicate that the resistances at stretching returned perfectly to their starting values, increased by approximately 8.5%, 25%, and 38% with respect to the initial resistance under 10%, 30%, and 50% strain, respectively. Therefore, prior to sensor assembly, a preconditioning step can be implemented, during which several cycles of stretching-releasing are applied, such that subsequent measurements will be reproducible. The GF values of the PS@Ag/PDMS-70 film at different strains after cycles are evaluated, as plotted in Fig. 4(b). It can be seen that few cycles are needed for the GF to stabilize under tensile strains. The GF values at strain of 10% are higher than that at 30% strain, but lower than that at 50% strain, which is attributed to the sudden resistance increase at low tensile strain, followed by alleviation under moderate strain and further increase due to the conductive paths being destroyed under large strain, which is consistent with the results shown in Fig. 3(a). For PS@Ag/PDMS-50, the normalized resistance and GF value at the maximum strain of 30% for stretching/releasing cycles are shown in Fig. 4(c). It can be seen that more cycles (15 cycles) are required for the normalized resistance and GF to stabilize than for the PS@Ag/PDMS-70 sensor. The GF value dramatically decreased from approximately 450 to 100; however, it is still a high sensitivity for a stretchable sensor. When the PS@Ag/PDMS-50 film was subjected to a maximum strain of 70% for stretching/releasing cycles, the normalized resistances showed a huge instability during the stretching/releasing cycles, especially in the first releasing stage, and showed an obvious hysteresis with each consecutive cycle, leading to a hysteresis that nearly spans over orders of magnitude for the cycles, as shown in Fig. 4(d). The results indicate

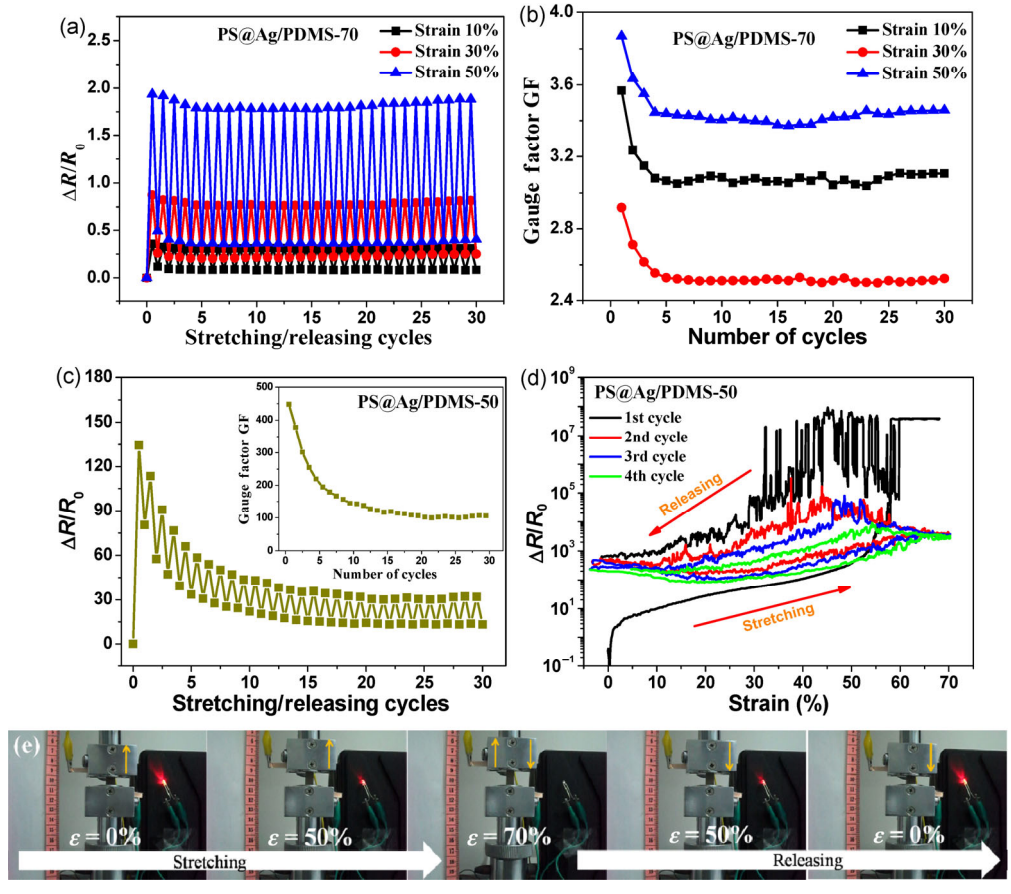

Figure 4 Multiple stretching/releasing cycle tests of change in resistance with different applied strains for (a) resistance variation after strain of 10%, 30%, 50% and then releasing for PS@Ag/PDMS-70, (b) GF value at strain of 10%, 30%, and 50% for each cycle for PS@Ag/PDMS-70. (c) Resistance variation after strain of 30% and then releasing for PS@Ag/PDMS-50. (d) Strain-dependent normalized resistance of PS@Ag/PDMS-50 under repeated stretching test. (e) Images of LED demonstration under repeated stretching/releasing cycles for PS@Ag/PDMS-50.

that a PS@Ag/PDMS sensor with low filler content near the percolation threshold, such as PS@Ag/PDMS-50, lacks reliability, making it unsuitable for use as precise sensor or actuator under high strain. Nevertheless, this remarkable change in resistance can be utilized for conductor–insulator cyclic transitions, which can be visually demonstrated by illuminating an LED, as shown in Fig. 4(e) and Video S2 in the ESM. The bulb gradually turned dim and turned off as the tensile strain increased to the maximum strain of rupture, and then gradually recovered brightness with the releasing of the strain to the initial level; this bright–dim transition can be well repeated under tensile cycles.

To understand the electrical property–strain dependency behavior observed above, SEM is carried out to investigate the inner morphology as well as the conductive networks structure in PS@Ag/PDMS composites during stretching, as shown in Figs. 5(a) and 5(b). It is observed that micron-sized PS@Ag conductive particles are homogeneously embedded in the insulating continuous PDMS phase at the untensile initial condition, i.e., ε = 0. When the sample is stretched, the relatively flat polymer phase becomes crumpled, and the distance between neighboring conductive spheres generally increases with increasing of strain parallel to the stretching direction. The conductivity of the composite is essentially decided by conductive network. For an intensive conductive network with high PS@Ag loading well above the percolation threshold, such as PS@Ag/PDMS-70, there exist enough conductive filler particles to connect with each other to form a multitude of different but

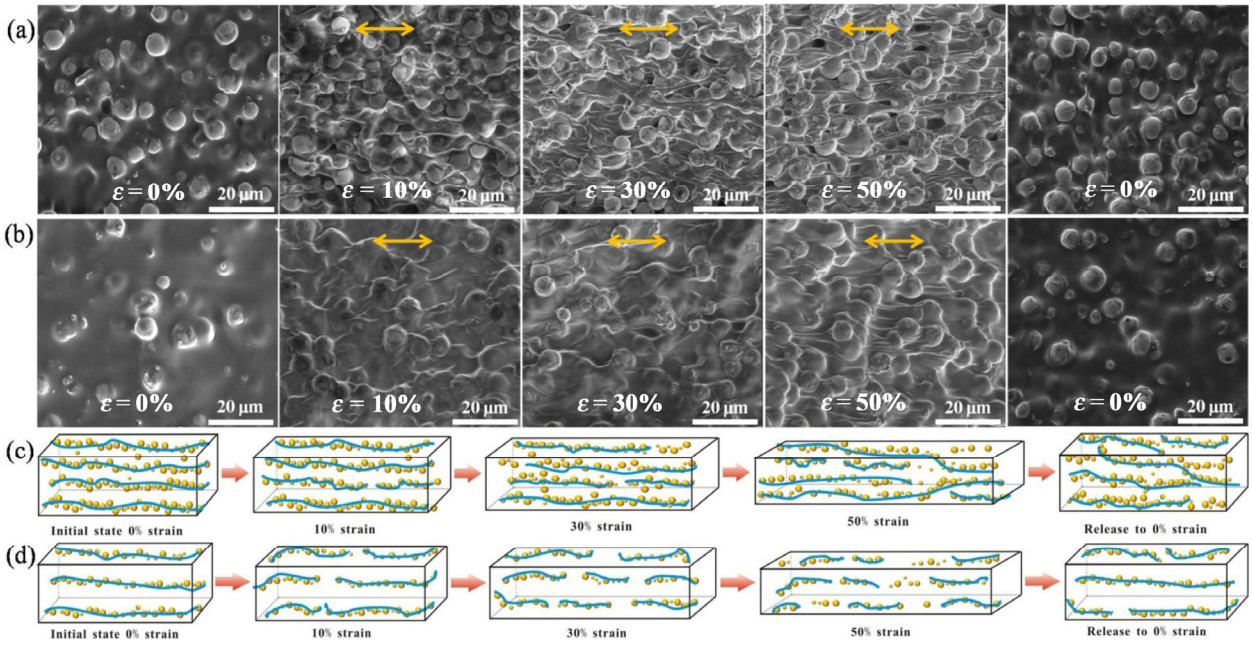

Figure 5 (a) and (b) SEM microscopic cross-sectional morphologies under various strains for PS@Ag/PDMS-70 and PS@Ag/PDMS-50, respectively. The brown arrows in the SEM images represent the stretching direction. (c) and (d) Schematic behavior of the PS@Ag/PDMS-70 and PS@Ag/PDMS-50 films during stretching, respectively.

similar complete conductive paths. When subjected to applied strains, a few conductive paths are broken down along the tensile direction. In the meantime, there may be created new conductive paths perpendicular to the strain direction due to the Poisson effect, leading to the total resistance showing a minor variation and repeatable resistance values within a large strain range. This also can be observed from Fig. 5(a), in which the conductive PS@Ag particles can be almost fully recovered to their respective initial state, which explains why the resistance is relatively stable after a few stretching/releasing cycles. The resistance of the PS@Ag/PDMS film after cycling is slightly increased as compared with its initial value, which can probably be ascribed to the rearrangement of the PS@Ag conductive networks and the decrease in the interface bonding between the filler particles and PDMS matrix. The changes in the conductive networks of PS@Ag/PDMS-70 under various stretching states are sketched in Fig. 5(c). However, for a sparse conductive filler distribution with low filler loading level only slightly more than the percolation threshold, such as PS@Ag/PDMS-50 (Fig. 5(b)), the composite only contains a small number of complete conductive paths. The conductivity of the composites is dominated by the tunneling resistance between local conductive networks. When subjected to tensile strain, even if at a relatively low level, the contact of conductive particles will be lost and the distance between conductive particles is likely to increase; the total resistance is expected to show a logarithmic relationship with strain owing to a lack of complete conductive paths, providing high sensitivity to small strains. Moreover, owing to low content of the PS@Ag conductive particles in the elastic PDMS matrix, it is hard to form new sufficient conductive networks when PS@Ag/PDMS sample is stretched, as shown in Fig. 5(d), ultimately resulting in a sharply increased resistance.

2.4 Application in printed interdigital electrode and stretchable conductive circuit

In view of their good conductivity, flexibility, and mechanical properties, the PS@Ag/PDMS elastic composites can be used for many flexible electronic devices. To evaluate the printability of the paste (uncured mixtures of PS@Ag particles and PDMS precursor), two typical "Chinese style" patterns of Chinese Knot and Panda were fabricated by screen-printing. As can

be seen from Figs. 6(a) and 6(b), the pretty and complicated patterns with trace width ranging from 0.3 to 0.5 mm are legible and distinguishable on paper substrate, demonstrating the printability and versatility of the paste. An array of nine interdigital electrode (IDE) units with total dimension of ~ 60 mm × 40 mm was successfully obtained on common paper substrate by screen-printing (Figs. 6(c)–6(f)). The printed IDE array can be used as a portable "on–off" switch that can be activated by an external conductor such as a metal weight. A blue LED was connected to the printed IDE array and power supplier. As can be seen in Fig. 6(c), before a weight touched the printed array, the LED is not functioning, indicating that no bridging between the adjacent printed PS@Ag/PDMS conductive traces occurred. When a stainless-steel weight of 1 g with diameter of 5 mm was randomly placed on the surface of one of the nine IDE units, the LED was on owing to the weight joining at least five neighboring printed conductive lines (Fig. 6(d)). When more weights were placed onto the printed IDE array, the luminance of the LED became brighter and brighter, as shown in Figs. 6(e) and 6(f) for two weights and three weights, respectively. This phenomenon can be explained by the fact that the contact areas between the printed IDEs and the conductive weights increase with increasing weight numbers, which results in decreasing of the contact resistance and ultimately increasing the LED brightness. The "on–off" working state of the printed IDEs array controlled by weight is also vividly demonstrated in Video S3 in the ESM. Moreover, a printed stretchable PS@Ag/PDMS conductive circuit with pentagram shape sandwiched by two PDMS layers was also fabricated by stencil printing. Ten LEDs connected into the printed circuit work well both under flat state (Fig. 6(g)) and intense curling state (Fig. 6(h)), large uniaxial stretching (Fig. 6(i)) and even biaxial stretching states (Fig. 6(j)). The results indicate that the PS@Ag/PDMS composite can perform as excellent and robust stretchable electrodes produced by a facile and efficient printing method.

2.5 Application in monitoring human motions

As mentioned previously, the PS@Ag/PDMS composites exhibit good stretchability and sensitivity, which can be used as strain sensors. For practical applications,

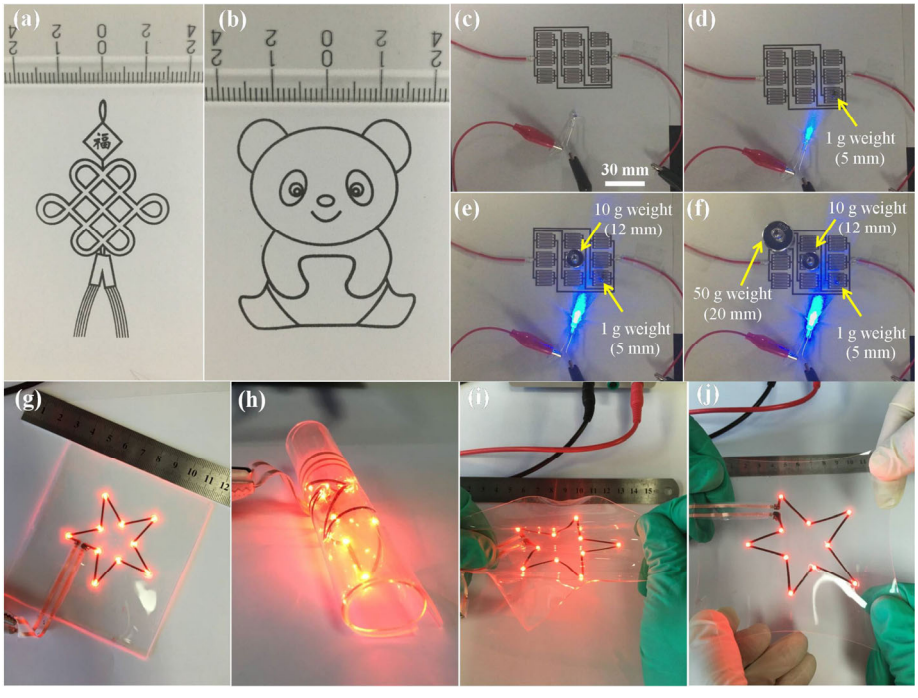

Figure 6 Demonstrations of the printability, stretchability, and conductivity of the PS@Ag/PDMS composites: (a) and (b) screen-printed images of Chinese Knot and Panda, respectively; (c)–(f) photographs of the flexible "on–off" switch fabricated by the printed IDE arrays under different working states; (g)–(j) photographs of the stretchable printed circuit under different deformations.

stability and durability are of great importance for the strain sensor. In order to alleviate the hysteresis and overshoot phenomenon, which is mainly caused by the viscoelastic nature of polymers as well as the interaction between the fillers and polymer matrix [32, 33], a sandwich structured PS@Ag/PDMS strain sensor was designed by embedding PS@Ag/PDMS between two layers of PDMS. The sandwich structure is an effective way to enhance the sensing quality, owing to the smaller hysteresis of the outer PDMS layers than that of the sealed PS@Ag/PDMS composites as shown in Fig. S2 in the ESM, which also has been proved by previous reports [23, 34]. To avoid a drastically decrease in sensitivity of the PS@Ag/PDMS composite as a sensor, asymmetric thicknesses of the PDMS layers, ~ 350 μm for the bottom substrate film and ~ 150 μm for the top seal layer, were used as shown in Fig. 7(a), because the bending leads to tension in one film and compression in the other film at the same time. If the thicknesses of the top and bottom layers were equal, the neutral point is placed at the center where the PS@Ag/PDMS composite is loaded [35]. Figure 7(b) demonstrates strong interface bonding between the PS@Ag/PDMS composite and the PDMS layers due to their similar components, which effectively avoids the delamination in the interface area during mechanical deformations of the strain sensor. The PS@Ag/PDMS and sandwich structured PS@Ag/PDMS strain sensors were stretched to strain of 30% and maintained for 90 s, the resistance of stretched sensors keep stable with overshoots of 23.02% and 14.67%, as shown in Fig. 7(c), respectively, manifesting a lower stress relaxation of the sandwich structured strain sensor than that of the simple PS@Ag/PDMS sensor. This result proves that the sandwich structure can improve the stable performance of the strain sensor.

Most electronic materials and devices are expected to heat up during operation from Joule heating and electromagnetic field radiation, among others. Therefore, we tested long term hydrothermal oxidation

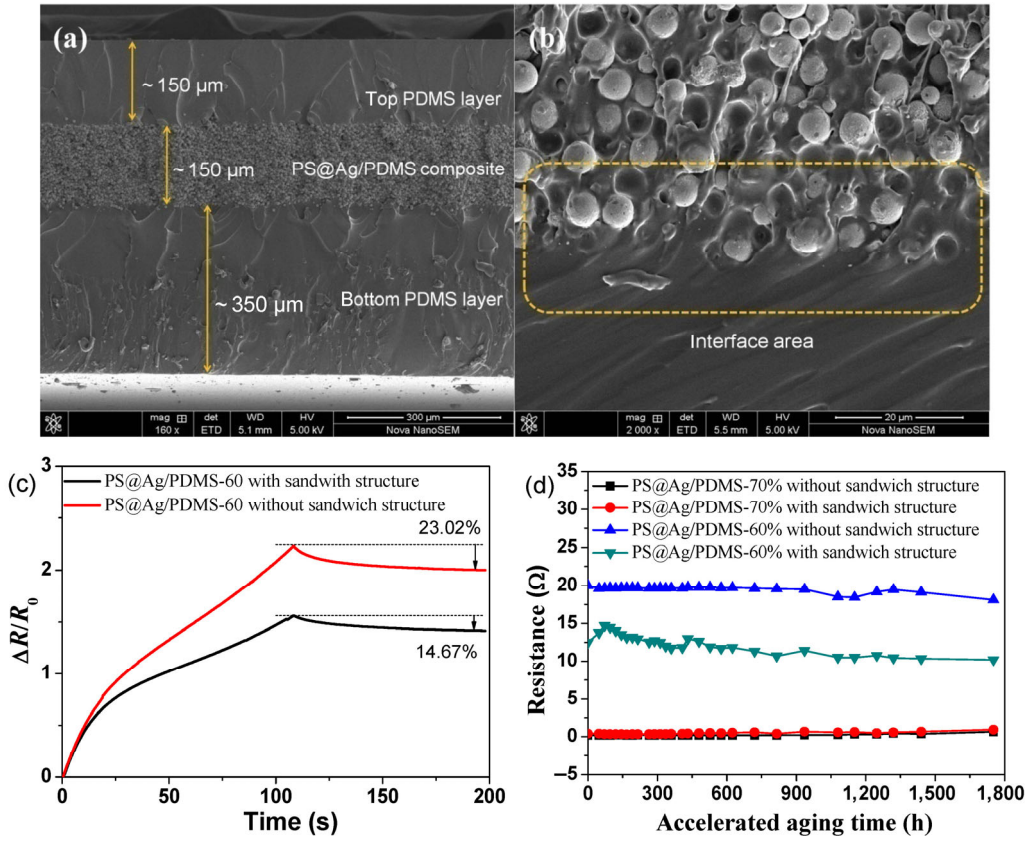

Figure 7 (a) and (b) Cross-sectional SEM images of the sandwich-structured PS@Ag/PDMS-60 strain sensor with low and high magnification, respectively. (c) Relative change in resistance versus time for increases in the strain from 0% to 30%. (d) Absolute resistance value as a function of aging time for PS@Ag/PDMS sensors after exposure to humid and hot air of 85 ˚C/85% RH.

stability of the PS@Ag/PDMS sensors by exposing them to the condition at 85 ℃ and 85% RH. Figure 7(d) shows the electrical property reliability against thermal oxidation time. It can be seen that there are no noticeable changes in resistance values after long-term aging tests (~ 1,750 h) for the two representative PS@Ag/PDMS-70 and PS@Ag/PDMS-60 sensors, regardless of whether they have a sandwich structure. The thermal–humidity aging test time for our sensors is significantly longer than that of 100 h for flexible silver nanowire electrodes [36], 504 h for conductive adhesives based on silver-coated polymer particles [37], and 1,000 h for electrically conductive composites based on silver micro/nanodendrites [38] in previous reports. The excellent long-term electrical stability of the PS@Ag/PDMS sensors after undergoing drastically accelerated environmental aging may be mainly attributed to the robust water vapor and oxygen gas barrier capability of the PDMS matrix and PDMS sealed layers, and also partly to the low level of silver loading in the conductive composites, which alleviates the oxidization of silver. It is believed that the PS@Ag/PDMS sensors both with and without sandwich structure represent an exciting prospect in flexible and wearable electronics, and can work effectively with high reliability for a much longer duration for practical applications.

To evaluate the applicability of the PS@Ag/PDMS composite used as strain sensor for monitoring human motion, a sandwich-structured PS@Ag/PDMS-60 strip is tested as a strain sensor for different body joints, such as the finger, wrist, and knee joints. In order to avoid slipping of the mounted sensor from the body joints, the sandwich structured sensor was attached to human index finger, wrist, and knee joints by tightly wrapping adhesive tape around the sensor electrodes. The resistance variation of the sensor was detected while the joints were repeatedly bent. As shown in Fig. 8(a), index finger bending motion can be easily reflected by the changes in the relative resistance $\Delta R/R_0$ of the strain sensor. During the full bending/relaxation motion, $\Delta R/R_0$ increases to the peak of approximately 1.0 ± 0.2 and nearly recovers to its original value, revealing the high sensitivity of the PS@Ag/PDMS sensor. This value is larger than those of many reported sensors applied to the

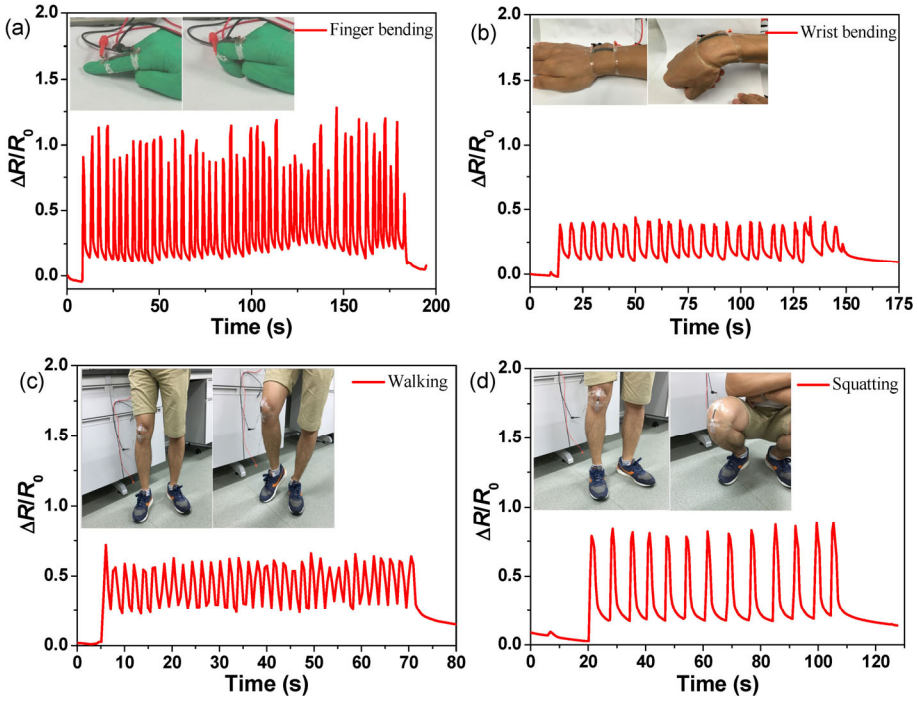

Figure 8 Monitoring of various human joint motions in real time. The changes in relative resistance of the sandwich-structured PS@Ag/PDMS sensor at ((a) and (b)) index finger and wrist for bending/relaxation motions, respectively. (c) and (d) Knee joint for various movements of walking and squatting, respectively.

same purpose of detecting finger bending, such as a graphene-based wool yarn sensor (10%–20%) [39], sandwich-structured AgNWs-PDMS nanocomposite strain sensor (10%–40%) [23], and fragmentized graphene foam (FGF)/PDMS sensor (50%–75%) [40]. The deviation of $\Delta R/R_0$ at maximum strain of the sensor is supposedly principally caused by the nonuniformity of finger bending motion (Video S4 in the ESM). The wrist bending motion was also detected by the sealed PS@Ag/PDMS-60 strain sensor, and the result is shown in Fig. 8(b). It can be seen that during bending/relaxation cycles of the wearer's wrist, $\Delta R/R_0$ is regularly increased to approximately 0.4 and rapidly recovers to the initial level with a slight increase. The smaller changes in the relative resistance during wrist bending motion compared with the finger bending motion can be attributed to smaller strain of the sensor during wrist bending than index finger bending, indicating that the PS@Ag/PDMS strain sensor can effectively distinguish different human body parts.

The knee is an important element of locomotion for a normal human, as well as the largest joint in the human body, which permits flexion and extension. Figures 8(c) and 8(d) present the sensing performance of the sandwich-structured PS@Ag/PDMS sensors mounted on a knee joint for walking and squatting (Video S5 in the ESM), respectively. As shown in Figs. 8(c) and 8(d), the sensor distinguishably responded to different motions owing to their different degrees of bending of the knee joint. When the wearer lifted his foot off the ground during walking or squatted down, the knee was flexed, causing the sensor to stretch and its resistance to increase. When the wearer returned to the standing posture, the knee extended, leading to the sensor recover and its relative resistance to decrease to its initial value. The $\Delta R/R_0$ peak values are approximately 0.6 and 0.8 for the walking and squatting states, respectively; both of these are larger than that of the wrist bending but smaller than that of the finger bending, indicating that the tensile strain of knee joint bending during walking and squatting is larger than that of wrist bending but smaller than that of index finger bending.

Furthermore, there is a short time period of about 1, 1, 0.5, and 1 for the sensor to reach peak resistance for the bending motions of the index finger, and wrist, and the flexing motions during walking and squatting down of the knee joint, respectively, indicating a fast response of the sensor (Fig. S4 in the ESM). The different times for each bending/relaxation motion of the finger, wrist, and knee can be ascribed to the different bending frequencies of the human body joints. The uniform signals during different human motions suggests good stability of the sensor. These results demonstrate that the PS@Ag/PDMS-based strain sensors possess an excellent combination of performance, including printability, high sensitivity, fast response, wide strain range, and good stability. Furthermore, they are able to monitor different human motions, and have promising potential in applications and devices such as e-skin and wearable electronic devices.

3 Conclusions

In conclusion, we reported a stretchable conductor and strain sensor based on PS@Ag/PDMS conductive elastic composites, which could be fabricated through a simple, low-cost, and scalable screen-printing process, and demonstrated its superior performance in flexible printed electrodes and monitoring vigorous human motions. To achieve feasible stretchability, resistance, and sensitivity, the PS@Ag conductive particle content in the elastic composites should be adjusted correctly. The PS@Ag/PDMS-60 strain sensor shows a wide workable strain range (> 80%), high sensitivity (GF of 17.5 at strains of 0%–10%, 6.0 at strains of 10%–60%, and 78.6 at strains of 60%–80%), as well as excellent long-term stability (1,750 h at 85 °C/85% RH). The excellent overall performance can be mainly ascribed to the percolation conductive network of the core–shell structured silver-coated polymer spheres. The sensing mechanism of the PS@Ag/PDMS strain sensor was verified by the tunneling theory. Its ability to monitor the movement of large joints in the human body such as finger, wrist, and knee joints was demonstrated. It is believed that the high-performance PS@Ag/PDMS conductive elastic composite has considerable potential for a wide variety of applications in next-generation all-soft electronics, such as flexible printed circuit boards and wearable electronic devices.

4 Experimental

4.1 Fabrication of PS@Ag/PDMS conductive film

Metallic silver-coated polystyrene sphere (PS@Ag) conductive particles with a size of 2–11 μm (average diameter of 5.68 μm) were synthesized by an improved electroless plating method, as described in our previous work [41]. The density of PS@Ag hybrid particles is 2.26 g/cm^3, and the Ag mass fraction in PS@Ag is ~ 61.2%. A homogenous conductive paste was prepared by vigorously mixing PS@Ag particles with a liquid silicone elastomer base and curing agent (Sylgard 184, Dow Corning) at a ratio of 10:1 by weight, and degassed under vacuum to remove the trapped air bubbles. The viscous conductive paste was cast into a polytetrafluoroethylene (PTFE) mold and scraped smooth to prepare the PS@Ag/PDMS conductive film and heat cured in a convection oven at 80 ℃ for 4 h followed by cutting into strips of desired sizes for further testing.

4.2 Fabrication of PS@Ag/PDMS interdigital electrode array and stretchable circuit

The PS@Ag/PDMS IDE array (consisting of nine interdigital electrodes, each electrode composed of 11 parallel lines with 10 mm line length, 0.5 mm line width, and 0.5 mm spacing) was printed by a screen-printing method using the PS@Ag/PDMS paste on a plain A4 paper substrate as a flexible "on–off" switch and cured at 80 ℃ for 4 h. The PS@Ag/PDMS stretchable circuit with pentacle shape was fabricated as follows. First, a half-cured PDMS substrate with a thickness ~ 200 μm was prepared by mixing the base and curing agent with a mass ratio of 10:1 and spin-coated at 300 rpm for 15 s on a Si wafer followed by curing at 60 ℃ for 30 min. Next, the conductive paste was printed onto this PDMS substrate by a stencil-printing process through a "five-point star" (17.8 mm length and 1 mm width for each line) metal shadow mask with a thickness of 100 μm. Ten LEDs and copper wires were then positioned into the printed PS@Ag/PDMS circuits, and they were baked in an oven at 70 ℃ for 30 min. Subsequently, another thin PDMS protecting layer was spin-coated on top of the printed circuit. Finally, the whole piece was thermally solidified at 80 ℃ for 2 h and peeled off from the Si wafer to obtain the printed PS@Ag/PDMS circuit sealed in two PDMS layers.

4.3 Fabrication of sandwich-structured strain sensor

Similar to the fabrication of the aforementioned stretchable circuit, the sandwich-structured PS@Ag/PDMS strain sensor was fabricated by screen-printing the conductive paste onto a half-cured PDMS substrate. After the copper electrodes were attached to the printed PS@Ag/PDMS traces, followed by curing in an oven at 70 ℃ for 1 h, another PDMS covering layer was spin-coated on the top of the printed traces and solidified at 80 ℃ for 2 h. The sample was cut into strips and carefully peeled off from the Si wafer to obtain the sandwich-structured PS@Ag/PDMS strain sensors (Fig. S5 in the ESM).

4.4 Characterization

The microscopic characteristics of samples were analyzed using field-emission scanning electron microscopy (FEI Nova Nano SEM 450). To observe the internal structure of the PS@Ag/PDMS films under strain, the specimens were clamped onto a customized sample stage under different elongations before observation. The mechanical property measurements of the PS@Ag/PDMS films were performed using an automatic electronic universal tester (RGM-4000) under a constant rate of 5 mm/min. The electrical resistance of the PS@Ag/PDMS films was examined by a two-probe method using a digital multimeter (Agilent 34401A). The resistivity can be calculated using the resistance by the following formula: $\rho = Rtw/l$, where R is the resistance of the sample, and t, w, and l represent the thickness, width, and length of the rectangular sample, respectively. The I–V characteristics of the PS@Ag/PDMS sensors were measured using a semiconductor characterization system (Keithley 4200-SCS) at room temperature. The accelerated aging test of the PS@Ag/PDMS sensors was carried out by storing them at 85 ℃/85% RH in a temperature and climatic test chamber (LP-150U) for 73 d. After the samples were dried in ambient conditions for 2 h, the resistance was measured at set intervals during the aging test period.

Acknowledgements

This work was supported by the National Key R&D Project from Minister of Science and Technology of China (No. 2016YFA0202702), National Natural Science Foundation of China (Nos. 61701488 and 21571186), Leading Scientific Research Project of Chinese Academy of Sciences (No. QYZDY-SSW-JSC010), Youth Innovation Promotion Association (No. 2017411), Guangdong Provincial Key Laboratory (No. 2014B030301014), Guangdong TeZhi Plan Youth Talent of Science and Technology (No. 2014TQ01C102), Shenzhen Basic Research plan (Nos. JSGG20150512145714246 and JSGG20160229155249762) and SIAT Innovation Program for Excellent Young Researchers (No. 2016005).

Electronic Supplementary Material: Supplementary material (the relationship between the mass fraction and volume fraction of PS@Ag fillers in the PS@Ag/PDMS composites, comparison of the percolation threshold, conductivity and sensing performance of electrically conductive composites, measurement of the Poisson's ratio of the PS@Ag/PDMS films, cyclic stress–strain curves of the PS@Ag/PDMS films, the GF values and the corresponding correlation coefficient R^2 of the linear fitting of PS@Ag/PDMS strain sensors, strain dependence of resistance for conductivity-invariant materials, experimental and theoretical data of strain-relative resistance dependence for PS@Ag/PDMS, magnified images of the changes in relative resistance of the sandwich-structured PS@Ag/PDMS-60 sensor, illustration of the fabrication process of the sandwich-structured PS@Ag/PDMS strain sensors, videos of the change of electrically conductive performance of PS@Ag/PDMS-65 and PS@Ag/PDMS-50, video of demonstration of the printed IDE arrays of PS@Ag/PDMS-60 and videos of wearable sensor of sandwich-structured PS@Ag/PDMS-60 in real-time monitoring of human motions) is available in the online version of this article at https://doi.org/10.1007/s12274-017-1811-0.

References

[1] Sekitani, T.; Noguchi, Y.; Hata, K.; Fukushima, T.; Aida, T.; Someya, T. A rubberlike stretchable active matrix using elastic conductors. *Science* **2008**, *321*, 1468–1472.

[2] Sekitani, T.; Nakajima, H.; Maeda, H.; Fukushima, T.; Aida, T.; Hata, K.; Someya, T. Stretchable active-matrix organic light-emitting diode display using printable elastic conductors. *Nat. Mater.* **2009**, *8*, 494–499.

[3] Mates, J. E.; Bayer, I. S.; Palumbo, J. M.; Carroll, P. J.; Megaridis, C. M. Extremely stretchable and conductive water-repellent coatings for low-cost ultra-flexible electronics. *Nat. Commun.* **2015**, *6*, 8874.

[4] Shi, J. D.; Li, X. M.; Cheng, H. Y.; Liu, Z. J.; Zhao, L. Y.; Yang, T. T.; Dai, Z. H.; Cheng, Z. G.; Shi, E. Z.; Yang, L. et al. Graphene reinforced carbon nanotube networks for wearable strain sensors. *Adv. Funct. Mater.* **2016**, *26*, 2078–2084.

[5] Oh, J. Y.; Kim, S.; Baik, H. K.; Jeong, U. Conducting polymer dough for deformable electronics. *Adv. Mater.* **2016**, *28*, 4455–4461.

[6] Roh, E.; Hwang, B.-U.; Kim, D.; Kim, B.-Y.; Lee, N.-E. Stretchable, transparent, ultrasensitive, and patchable strain sensor for human-machine interfaces comprising a nanohybrid of carbon nanotubes and conductive elastomers. *ACS Nano* **2015**, *9*, 6252–6261.

[7] Wang, Y.; Yang, T. T.; Lao, J. C.; Zhang, R. J.; Zhang, Y. Y.; Zhu, M.; Li, X.; Zhang, X. B.; Wang, K. L.; Yu, W. J. et al. Ultra-sensitive graphene strain sensor for sound signal acquisition and recognition. *Nano Res.* **2015**, *8*, 1627–1636.

[8] Lee, S.; Shin, S.; Lee, S.; Seo, J.; Lee, J.; Son, S.; Cho, H. J.; Algadi, H.; Al-Sayari, S.; Kim, D. E. et al. Ag nanowire reinforced highly stretchable conductive fibers for wearable electronics. *Adv. Funct. Mater.* **2015**, *25*, 3114–3121.

[9] Kim, D. H.; Lu, N. S.; Ma, R.; Kim, Y. S.; Kim, R. H.; Wang, S. D.; Wu, J.; Won, S. M.; Tao, H.; Islam, A. et al. Epidermal electronics. *Science* **2011**, *333*, 838–843.

[10] Tee, B. C.-K.; Wang, C.; Allen, R.; Bao, Z. N. An electrically and mechanically self-healing composite with pressure- and flexion-sensitive properties for electronic skin applications. *Nat. Nanotechnol.* **2012**, *7*, 825–832.

[11] You, I.; Kim, B.; Park, J.; Koh, K.; Shin, S.; Jung, S.; Jeong, U. Stretchable e-skin apexcardiogram sensor. *Adv. Mater.* **2016**, *28*, 6359–6364.

[12] Martinez, R. V.; Branch, J. L.; Fish, C. R.; Jin, L. H.; Shepherd, R. F.; Nunes, R. M. D.; Suo, Z. G.; Whitesides, G. M. Robotic tentacles with three-dimensional mobility based on flexible elastomers. *Adv. Mater.* **2013**, *25*, 205–212.

[13] Matsuhisa, N.; Kaltenbrunner, M.; Yokota, T.; Jinno, H.; Kuribara, K.; Sekitani, T.; Someya, T. Printable elastic conductors with a high conductivity for electronic textile applications. *Nat. Commun.* **2015**, *6*, 7461.

[14] Wu, C. X.; Kim, T. W.; Li, F. S.; Guo, T. L. Wearable electricity generators fabricated utilizing transparent electronic textiles based on polyester/Ag nanowires/graphene core–shell nanocomposites. *ACS Nano* **2016**, *10*, 6449–6457.

[15] Lai, Y. C.; Ye, B. W.; Lu, C. F.; Chen, C. T.; Jao, M. H.; Su,

W. F.; Hung, W. Y.; Lin, T. Y.; Chen, Y. F. Extraordinarily sensitive and low-voltage operational cloth-based electronic skin for wearable sensing and multifunctional integration uses: A tactile-induced insulating-to-conducting transition. *Adv. Funct. Mater.* **2016**, *26*, 1286–1295.

[16] Yamada, T.; Hayamizu, Y.; Yamamoto, Y.; Yomogida, Y.; Izadi-Najafabadi1, A.; Futaba, D. N.; Hata, K. A stretchable carbon nanotube strain sensor for human-motion detection. *Nat. Nanotechnol.* **2011**, *6*, 296–301.

[17] Gao, W.; Emaminejad, S.; Nyein, H. Y. Y.; Challa, S.; Chen, K.; Peck, A.; Fahad, H. M.; Ota, H.; Shiraki, H.; Kiriya, D. et al. Fully integrated wearable sensor arrays for multiplexed *in situ* perspiration analysis. *Nature* **2016**, *529*, 509–514.

[18] Trung, T. Q.; Lee, N.-E. Flexible and stretchable physical sensor integrated platforms for wearable human-activity monitoring and personal healthcare. *Adv. Mater.* **2016**, *28*, 4338–4372.

[19] Fan, F. R.; Tang, W.; Wang, Z. L. Flexible nanogenerators for energy harvesting and self-powered electronics. *Adv. Mater.* **2016**, *28*, 4283–4305.

[20] Ryu, S.; Lee, P.; Chou, J. B.; Xu, R. Z.; Zhao, R.; Hart, A. J.; Kim, S. G. Extremely elastic wearable carbon nanotube fiber strain sensor for monitoring of human motion. *ACS Nano* **2015**, *9*, 5929–5936.

[21] Yoon, S. G.; Koo, H. J.; Chang, S. T. Highly stretchable and transparent microfluidic strain sensors for monitoring human body motions. *ACS Appl. Mater. Interfaces* **2015**, *7*, 27562–27570.

[22] Fan, J. A.; Yeo, W. H.; Su, Y. W.; Hattori, Y.; Lee, W.; Jung, S.-Y.; Zhang, Y. H.; Liu, Z. J.; Cheng, H. Y.; Falgout, L. et al. Fractal design concepts for stretchable electronics. *Nat. Commun.* **2014**, *5*, 3266.

[23] Amjadi, M.; Pichitpajongkit, A.; Lee, S.; Ryu, S.; Park, I. Highly stretchable and sensitive strain sensor based on silver nanowire-elastomer nanocomposite. *ACS Nano* **2014**, *8*, 5154–5163.

[24] Song, H. L.; Zhang, J. Q.; Chen, D. B.; Wang, K. J.; Niu, S. C.; Han, Z. W.; Ren, L. Q. Superfast and high-sensitivity printable strain sensors with bioinspired micron-scale cracks. *Nanoscale* **2017**, *9*, 1166–1173.

[25] Stauffer, D.; Aharony, A. *Introduction to Percolation Theory*; 2nd ed. London: Taylor and Francis: London, 1992.

[26] Weber, M.; Kamal, M. R. Estimation of the volume resistivity of electrically conductive composites. *Polym. Compos.* **1997**, *18*, 711–725.

[27] Larmagnac, A.; Eggenberger, S.; Janossy, H.; Voros, J. Stretchable electronics based on Ag-PDMS composites. *Sci. Rep.* **2014**, *4*, 7254.

[28] Hu, G. J.; Zhao, C. G.; Zhang, S. M.; Yang, M. S.; Wang, Z. G. Low percolation thresholds of electrical conductivity and rheology in poly(ethylene terephthalate) through the networks of multi-walled carbon nanotubes. *Polymer* **2006**, *47*, 480–488.

[29] Dorfmann, A.; Ogden. R. W. A constitutive model for the mullins effect with permanent set in particle-reinforced rubber. *Int. J. Solids Struct.* **2004**, *41*, 1855–1878.

[30] Simmons, J. G. Electric tunnel effect between dissimilar electrodes separated by a thin insulating film. *J. Appl. Phys.* **1963**, *34*, 2581–2590.

[31] Chen, L.; Chen, G. H.; Lu, L. Piezoresistive behavior study on finger-sensing silicone rubber/graphite nanosheet nanocomposites. *Adv. Funct. Mater.* **2007**, *17*, 898–904.

[32] Alamusi; Hu, N.; Fukunaga, H.; Atobe, S.; Liu, Y. L.; Li, J. H. Piezoresistive strain sensors made from carbon nanotubes based polymer nanocomposites. *Sensors* **2011**, *11*, 10691–10723.

[33] Kong, J. H.; Jang, N. S.; Kim, S. H.; Kim, J. M. Simple and rapid micropatterning of conductive carbon composites and its application to elastic strain sensors. *Carbon* **2014**, *77*, 199–207.

[34] Jeon, J. Y.; Ha, T. J. Waterproof electronic-bandage with tunable sensitivity for wearable strain sensors. *ACS Appl. Mater. Interfaces* **2016**, *8*, 2866–2871.

[35] Takei, K.; Yu, Z. B.; Zheng, M.; Ota, H.; Takahashi, T.; Javey, A. Highly sensitive electronic whiskers based on patterned carbon nanotube and silver nanoparticle composite films. *Proc. Natl. Acad. Sci. USA* **2014**, *111*, 1703–1707.

[36] Jang, J.; Im, H. G.; Jin, J.; Lee, J.; Lee, J. Y.; Bae, B. S. A flexible and robust transparent conducting electrode platform using an electroplated silver grid/surface-embedded silver nanowire hybrid structure. *ACS Appl. Mater. Interfaces* **2016**, *8*, 27035–27043.

[37] Pettersen, S. R.; Kristlansen, H.; Nagao, S.; Helland, S.; Niagi, J.; Suganuma, K.; Zhang, Z. L.; He, J. Y. Contact resistance and metallurgical connections between silver coated polymer particles in isotropic conductive adhesives. *J. Electron. Mater*. 2016, *45*, 3734–3743.

[38] Yang, R.; Wang, Y.; Wu, D.; Deng, Y. B.; Luo, Y. Y.; Cui, X. Y.; Wang, X. Y.; Shu, Z. X.; Yang, C. Low-temperature fusible silver micro/nanodendrites-based electrically conductive composites for next-generation printed fuse-links. *ACS Nano*, **2017**, *11*, 7710–7718.

[39] Park, J. J.; Hyun, W. J.; Mun, S. C.; Park, Y. T.; Park, O. O. Highly stretchable and wearable graphene strain sensors with controllable sensitivity for human motion monitoring. *ACS Appl. Mater. Interfaces* **2015**, *7*, 6317–6324.

[40] Jeong, Y. R.; Park, H.; Jin, S. W.; Hong, S. Y.; Lee, S. S.; Ha, J. S. Highly stretchable and sensitive strain sensors using fragmentized graphene foam. *Adv. Funct. Mater.* **2015**, *25*, 4228–4236.

[41] Hu, Y. G.; Zhao, T.; Zhu, P. L.; Zhu, Y.; Shuai, X. T.; Liang, X. W.; Sun, R.; Lu, D. D.; Wong, C. P. Low cost and highly conductive elastic composites for flexible and printable electronics. *J. Mater. Chem. C* **2016**, *4*, 5839–5848.